

# ***An Investigation of the Reliability of the Taiwan Earthquake Model PSHA2015***

**by Yu-Ju Wang, Ya-Ting Lee, Chung-Han Chan, and Kuo-Fong Ma**

## **ABSTRACT**

The Taiwan Earthquake Model (TEM) has had a new probabilistic seismic-hazard analysis (PSHA) model for determining the probability of exceedance (PoE) of the ground motion over a specified period in Taiwan. We conducted several tests to investigate the adequacy of the seismic source parameters adopted by the TEM in 2015 (TEM PSHA2015). The observed maximal peak ground accelerations (PGAs) of the  $M_L > 4.0$  mainshocks from 1993 to 2015 were used to test the predicted PGA from areal and subduction zone sources based on a time-independent Poisson distribution. This comparison excluded the observations from the 1999 Chi-Chi earthquake, because this was the only earthquake associated with the identified active fault in the testing period. We used tornado diagrams to analyze the sensitivities of these source parameters to the ground-motion values of the PSHA. This study showed that the predicted PGA for a 63% PoE in the 23-year period corresponded to observations, confirming the applicability of the parameters to areal and subduction zone sources. We adopted disaggregation analysis to determine the contribution of each seismic source to the hazard for six metropolitan cities in Taiwan. Sensitivity tests on the seismogenic structure parameters indicated that slip rate and maximum magnitude are the dominant factors in the TEM PSHA2015. For densely populated faults in southwestern Taiwan, the assessed hazard level is more sensitive to the maximum magnitude of earthquakes than it is to the slip rate of active faults, creating concern for the possibility of larger earthquakes due to multiple-segment ruptures in this area, which has not yet been considered in the TEM PSHA2015. The source category disaggregation also suggested a seismic hazard over long periods in northern Taiwan due to subduction zone sources.

## **INTRODUCTION**

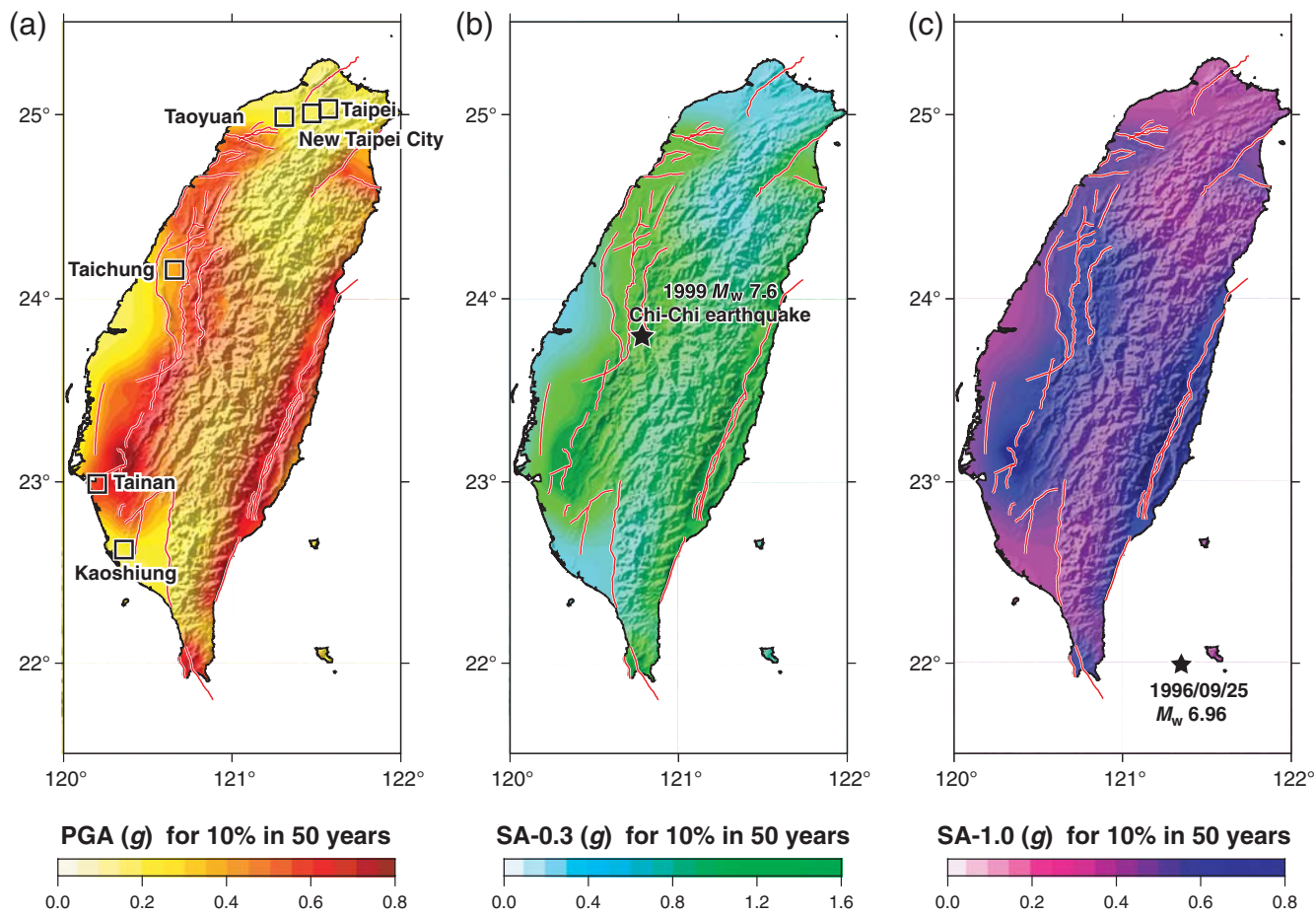
A probabilistic seismic-hazard analysis (PSHA; [Cornell, 1968](#)) determines the probability of exceedance (PoE) for various levels of ground motion over a specified period. PSHAs are key references in mitigating seismic risk, with applications such as building code legislation development, site selection for public and private infrastructure, and insurance premium calculation. Therefore, numerous organizations have attempted to develop a reliable PSHA at different spatial scales (e.g., [Giardini \*et al.\*, 1999](#); [SHARE, 2013](#); [J-SHIS, 2015](#)). In Taiwan, the

Taiwan Earthquake Model (TEM) assessed the seismic hazard in 2015 and proposed hazard maps in the forms of peak ground acceleration (PGA), spectral acceleration at 0.3 s (SA-0.3) and spectral acceleration at 1.0 s (SA-1.0) ([Fig. 1](#); [Wang \*et al.\*, 2016](#)).

PSHAs include epistemic and aleatoric uncertainties ([Senior Seismic Hazard Analysis Committee, 1997](#)). The epistemic uncertainty is scientific uncertainty caused by a lack of knowledge or data. For example, a catalog with a short record renders an unclear understanding of earthquake behaviors. The aleatoric uncertainty represents natural randomness, which is difficult to minimize. The development of a more precise PSHA model requires minimizing the uncertainties through clarifying the significance of each uncertainty factor.

Disaggregation and parameter sensitivity tests are common tools for quantifying PSHA uncertainties ([Bazzurro and Cornell, 1999](#); [Rebez and Slejko, 2000](#); [Giner \*et al.\*, 2002](#); [Beauval and Scotti, 2004](#); [Albarelo and D'Amico, 2008](#); [Stein \*et al.\*, 2015](#)). Disaggregation helps in understanding the contribution of each seismogenic source to the hazard, and parameter sensitivity tests estimate the uncertainties in the input parameters which affect the deviation in the hazard. We adopted disaggregation analysis from a hazard map to determine the contributions of the individual seismic sources to the hazard for six metropolitan cities (squares in [Fig. 1a](#)). We conducted a series of sensitivity tests on source parameters to justify the practicability of the TEM PSHA2015.

Comparing the expected ground-motion levels with the observed ones could be used to examine the practicability of a PSHA model ([Albarelo and D'Amico, 2008](#); [Beauval \*et al.\*, 2008, 2010](#); [Miyazawa and Mori, 2009](#); [Stirling and Gerstenberger, 2010](#); [Tasan \*et al.\*, 2014](#)). [Mak and Schorlemmer \(2016\)](#) compared the seismic-hazard forecasts of the four published versions of the U.S. Geological Survey National Seismic Hazard Maps with observed ground motion. Their results show that the observations were found to be generally consistent with the forecasts. The predicted ground shaking from the TEM PSHA2015 was compared with instrumental observations since 1993. The TEM PSHA2015 was under the Poisson assumption, in which the event rupture probability in a fixed interval of time and space is the same for different time windows as a time-independent model. Thus, an expected value of PGA could be observed during the observational time window.



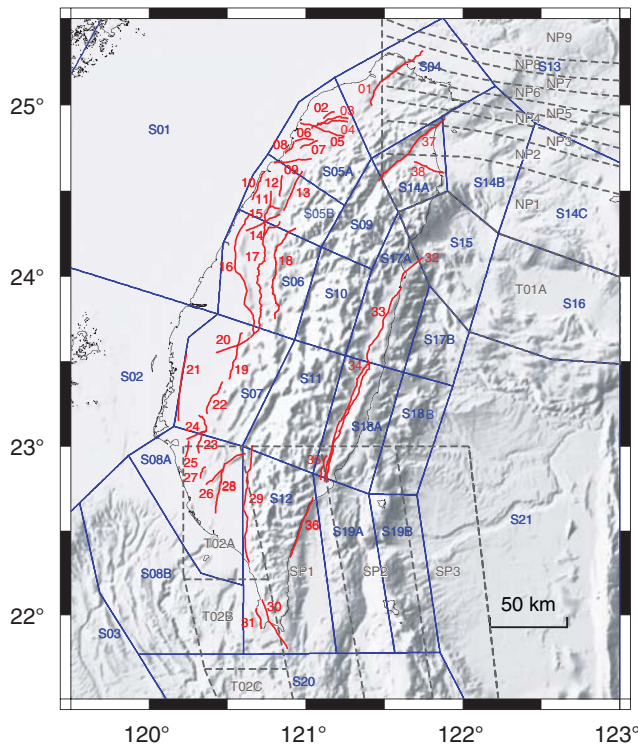
▲ **Figure 1.** Hazard maps of the Taiwan Earthquake Model (TEM) PSHA2015 (Wang *et al.*, 2016) for (a) peak ground acceleration (PGA), (b) spectral acceleration at 0.3 s (SA-0.3), and (c) spectral acceleration at 1.0 s (SA-1.0) for 10% probability of exceedance (PoE) in 50 years (corresponding to a recurrence interval of 475 years). The squares denote the six metropolitan cities analyzed in this study. The star in (b) shows the location of the 1999 Chi-Chi earthquake. The star in (c) shows the location of the recorded maximal magnitude from an areal source of the 5 September 1996  $M_w$  6.96 southeast offshore Taiwan earthquake.

### TEM PSHA2015

The TEM PSHA2015 (Wang *et al.*, 2016) implements up-to-date parameters for crustal, which are the seismogenic structure sources including both active and blind faults (Shyu *et al.*, 2016; Table 1) and areal sources (Table 2), as well as subduction zone sources (Fig. 2; Table 3) under the assumption of a Poisson distribution. We refer to seismogenic structure sources rather than active fault sources, as the seismogenic structure sources include frontal structures and blind faults without surface rupture. The areal source refers to the seismicity, which cannot be associated with any identified seismogenic structure source. Overall, this model represents the seismogenic structure sources that dominate the seismic hazard (Fig. 1). The maximum magnitude of the seismogenic structures was estimated on the basis of the fault length and width by the scaling law of Wells and Coppersmith (1994; Table 1). The TEM PSHA2015 considers the characteristic earthquakes on seismogenic structures and the compiled and examined slip rates of each seismogenic structure by Shyu *et al.* (2016) to infer the corresponding recurrence intervals. For the areal sources, we

applied the frequency–magnitude distributions of the seismicity to infer the recurrence of the earthquakes. The rate distributions were modeled based on the catalog recorded by the Taiwan Central Weather Bureau (CWB) during 1973–2011 and declustered using the algorithm of Gardner and Knopoff (1974). The TEM PSHA2015 was calculated using an estimated value for each source parameter; that is, a logic tree for source parameters is not implemented and parameter uncertainty is not discussed. To evaluate the ground shaking attenuation, the ground-motion prediction equations (GMPEs) of Lin (2009) and Lin and Lee (2008) are applied to crustal and subduction sources, respectively. The TEM PSHA2015 was computed for bedrock sites ( $V_{s30} = 760$  m/s) to provide a basis for crucial infrastructures and flexibility for forthcoming models to consider the site response. Based on the parameter setting, the predicted ground motion is expected to be time independent.

The hazard map of the TEM PSHA2015 (Fig. 1; Wang *et al.*, 2016) shows that the regions near seismogenic structures with large maximal magnitudes or/and high slip rates (Table 1) have high seismic hazards, including Tainan near the Chungchou



▲ **Figure 2.** Seismic sources adopted in the hazard map of the TEM PSHA2015. The 28 subregions of the areal sources are delineated by the blue lines, the 38 seismogenic structures (Shyu *et al.*, 2016) are indicated by the red lines, and the subregions of the subduction zone sources for interplate (T) and intraplate earthquake sources (SP and NP) are delineated by the dashed gray lines.

structure (ID 23, Fig. 2), the southern tip of Taiwan near the Hengchun fault (ID 30, Fig. 2), the eastern Taiwan along the Milun fault (ID 32, Fig. 2), and the longitudinal valley fault (ID 33, Fig. 2). In contrast, aseismic zones (e.g., the central ranges in S09, Fig. 2) and regions with less seismicity (e.g., northern Taiwan in S04 and S05A) have low seismic-hazard levels.

## PSHA MODEL DISAGGREGATION FOR SIX METROPOLITAN CITIES

Figure 3 shows the source category disaggregation of the TEM PSHA2015 for six metropolitan cities (squares in Fig. 1a) for ground shaking in the forms of PGA, spectral acceleration at 0.3 s (SA-0.3), and spectral acceleration at 1.0 s (SA-1.0). The hazard was principally contributed from the crustal sources, that is, the areal sources and seismogenic structures, although intraplate sources, also contributed some hazard to Taipei and New Taipei City. The disaggregation provided an overview of the dominant seismic sources contributing to the seismic hazard in the six cities. In our PSHA, the ground-motion levels were evaluated based on the earthquake magnitude and source-to-site distance characterized by GMPEs. To comprehend the PSHA deviation from source and path, the magnitude-distance-epsilon ( $\epsilon$ ) disaggregation values for the six cities are

represented (Fig. 4). They show that the  $-1$  to 2 standard deviation of the GMPE estimation would have significant contribution to the hazards of the six cities. In the northern Taiwan cities (i.e., Taipei, New Taipei City, and Taoyuan), the hazard contributions could be from the source distance 100 km away from the site. The dominant magnitudes in Taipei and New Taipei City were  $\sim 7.0$ , consistent with the maximum magnitude on the Shanchiao fault (ID 1, Fig. 2). In Taoyuan, the hazard came from near-field sources with magnitudes of 6.0–7.5, corresponding to the Shanchiao, Shuanglienpo, Yangmei, and Hukou faults (ID 1–4, respectively, Fig. 2). For the cities in central and southern Taiwan (Fig. 4d–f), the distances to the dominant sources are short (0–20 km). In Taichung, the seismic hazard was mainly contributed by earthquakes with magnitudes greater than 7.0, which could be attributed to the relatively lengthy faults in central Taiwan. In Tainan, the seismic hazard was dominated by magnitude 6.0 earthquakes, and the dominant earthquake magnitude was 6.0–7.0 in Kaohsiung due to the shorter faults in the vicinity. The disaggregation analysis provided an overview of the hazard contributions to the target sites, revealing a strong correlation between faults and hazards.

The above analysis shows seismic hazard from intraplate subduction zone events in northern cities, but a limited contribution from interplate subduction zone earthquakes. Note that due to the lack of knowledge on the Ryukyu and Manila subduction zones, the assumptions of the maximum magnitudes considered in the current model for the two sources might depart from reality. The high uncertainty could exist in  $M_{\max}$  of interplate earthquakes. Unfortunately, using the knowledge obtained to date and the limited data at hand, we are still not able to quantify a seismic hazard of this type. However, the disaggregation analysis of the northern cities also gives hints as to the potential hazard from a megathrust earthquake on the subduction slab. To quantify  $M_{\max}$  of the interplate subduction zone events and their associated probability is indeed essential and will be addressed in our next TEM PSHA model.

## COMPARISON WITH OBSERVED PGA FOR AREAL AND SUBDUCTION SOURCES

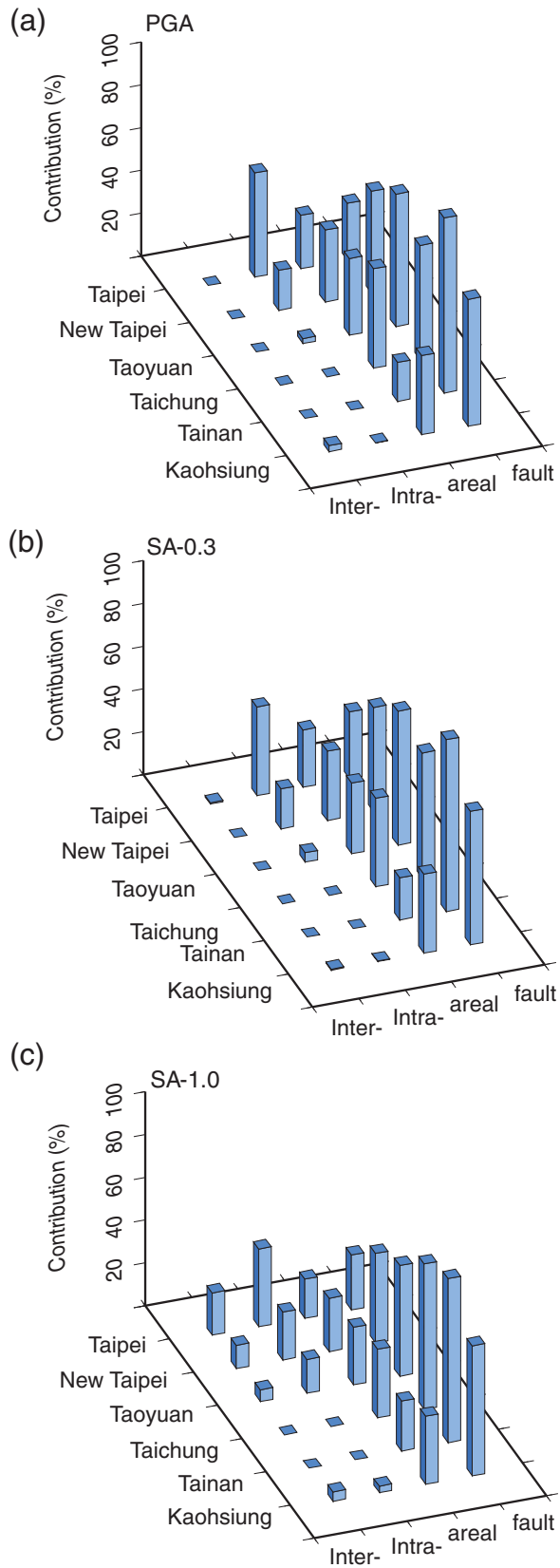
The TEM PSHA2015 was based on the Poisson process (Cornell, 1968), in which the probability is assumed to be time independent (i.e., constant over time). In this study, we investigated and tested the TEM PSHA2015 for crustal and subduction zone sources. However, for crustal sources, we tested the PSHA only for the areal source, as seismogenic structure sources are associated with characteristic earthquakes, the time elapsed since the last event has not yet been verified.

The seismicity rates of areal sources adopted in the TEM PSHA2015 were parameterized with the recorded events during 1973–2011 (Wang *et al.*, 2016), as a more complete seismic catalog was compiled after 1973 (Chen *et al.*, 2013). Since 1993, the CWB established more than 700 stations for the Taiwan Strong Motion Instrumentation Program (TSMIP), which has recorded thousands of earthquakes with  $M_L > 4.0$ . During

**Table 1**  
**Source Parameters of the 38 Seismogenic Structures Utilized in Taiwan Earthquake Model (TEM) PSHA2015 (Wang *et al.*, 2016)**  
**with Deviation Adopted in the Tornado Diagrams**

ID	Name	Type	Area (km <sup>2</sup> )	Dip (°)	Maximum <i>M<sub>w</sub></i> (W & C)	Slip Rate (mm/yr)	Maximum	Maximum
							<i>M<sub>w</sub></i> (Y & M) Strike/Dip Slip	<i>M<sub>w</sub></i> (Y & M) All Events
1	Shanchiao fault	N	1059.46	60 (±10%)	7.0 (±0.2)	1.85 (±0.76)	6.8	6.8
2	Shuanglienpo structure	R	107.73	45 (±10%)	6.2 (±0.2)	0.25 (±0.17)	6.0	6.1
3	Yangmei structure	R	75.08	60 (±10%)	6.0 (±0.2)	0.38 (±0.26)	5.9	5.9
4	Hukou fault	R	516.00	30 (±10%)	6.8 (±0.2)	1.16 (±0.84)	6.6	6.6
5	Fengshan River strike-slip structure	SS	422.56	85 (±10%)	6.7 (±0.2)	3.61 (±2.41)	6.5	6.5
6	Hsinchu fault	R	178.16	45 (±10%)	6.4 (±0.2)	0.70 (±0.46)	6.2	6.2
7	Hsincheng fault	R	334.23	30 (±10%)	6.6 (±0.2)	1.80 (±1.20)	6.4	6.4
8	Hsinchu frontal structure	R	208.00	30 (±10%)	6.4 (±0.2)	2.80 (±1.86)	6.2	6.3
9	Touhuanping structure	SS	298.84	85 (±10%)	6.5 (±0.2)	0.14	6.4	6.4
10	Miaoli frontal structure	R	416.00	30 (±10%)	6.7 (±0.2)	3.60 (±2.40)	6.5	6.5
11	Tunglo structure	R	77.70	30 (±10%)	6.0 (±0.2)	1.08 (±0.72)	5.9	5.9
12	East Miaoli structure	R	112.80	30 (±10%)	6.2 (±0.2)	1.60 (±1.06)	6.0	6.1
13	Shihtan fault	R	319.75	75 (±10%)	6.6 (±0.2)	1.86 (±1.24)	6.4	6.4
14	Sanyi fault	R	945.74	15 (±10%)	7.0 (±0.2)	1.86 (±1.23)	6.8	6.8
15	Tuntzuchiaofault	SS	372.74	85 (±10%)	6.6 (±0.2)	1.00 (±0.68)	6.5	6.5
16	Changhua fault	R	4180.15	45 (±10%)	7.6 (±0.2)	3.40 (±2.26)	7.3	7.3
17	Chelungpu fault	R	4265.12	15 (±10%)	7.6 (±0.2)	6.94	7.3	7.3
18	Tamaopu-Shuangtung fault	R	824.40	30 (±10%)	7.0 (±0.2)	2.00 (±1.34)	6.7	6.7
19	Chiuchungkeng fault	R	789.60	30 (±10%)	6.9 (±0.2)	7.20 (±4.80)	6.7	6.7
20	Meishan fault	SS	354.00	85 (±10%)	6.6 (±0.2)	2.51	6.5	6.5
21	Chiayi frontal structure	R	2053.75	15 (±10%)	7.3 (±0.2)	6.49 (±4.33)	7.1	7.0
22	Muchiliao–Liuchia fault	R	597.60	30 (±10%)	6.8 (±0.2)	5.75 (±1.35)	6.6	6.6
23	Chungchou structure	R	712.80	30 (±10%)	6.9 (±0.2)	12.20 (±0.60)	6.7	6.7
24	Hsinhua fault	SS	212.35	85 (±10%)	6.4 (±0.2)	2.65 (±1.85)	6.3	6.3
25	Houchiali fault	R	81.31	45 (±10%)	6.1 (±0.2)	7.07	5.9	6.0
26	Chishan fault	SS/R	389.06	75 (±10%)	6.6 (±0.2)	1.10 (±0.36)	6.5	6.5
27	Hsiaokangshan fault	R	126.00	30 (±10%)	6.2 (±0.2)	3.30 (±2.20)	6.1	6.1
28	Kaoping River structure	SS/R	371.13	75 (±10%)	6.6 (±0.2)	0.61 (±0.41)	6.5	6.5
29	Chaozhou fault	SS/R	915.40	75 (±10%)	7.0 (±0.2)	1.76 (±1.17)	6.8	6.8
30	Hengchun fault	SS/R	577.72	75 (±10%)	6.8 (±0.2)	6.15 (±0.29)	6.6	6.6
31	Hengchun offshore structure	R	116.00	30 (±10%)	6.2 (±0.2)	3.65 (±1.11)	6.0	6.1
32	Milun fault	SS/R	220.46	75 (±10%)	6.4 (±0.2)	10.15 (±0.04)	6.3	6.3
33	Longitudinal valley fault	R/SS	3404.35	75 (±10%)	7.5 (±0.2)	11.35 (±5.75)	7.3	7.2
34	Central range structure	R	2417.94	45 (±10%)	7.4 (±0.2)	7.28 (±1.77)	7.1	7.1
35	Luyeh fault	R	119.52	45 (±10%)	6.2 (±0.2)	6.34 (±0.17)	6.0	6.1
36	Taimali coastline structure	R/SS	465.62	75 (±10%)	6.7 (±0.2)	7.32 (±1.46)	6.5	6.5
37	Northern Ilan structure	N	657.64	60 (±10%)	6.8 (±0.2)	3.29 (±2.25)	6.7	6.7
38	Southern Ilan structure	N	267.59	60 (±10%)	6.4 (±0.2)	5.48 (±0.64)	6.3	6.4

Maximum magnitudes estimated by scaling laws of [Yen and Ma \(2011\)](#) for dip-slip events, strike-slip events, and all events collectively are also listed (denoted by Y & M). The values in brackets show the deviation adopted in the tornado diagram. Fault types: R, reverse slip; SS, strike slip; N, normal slip. W & C, values estimated using the scaling laws of [Wells and Coppersmith \(1994\)](#).

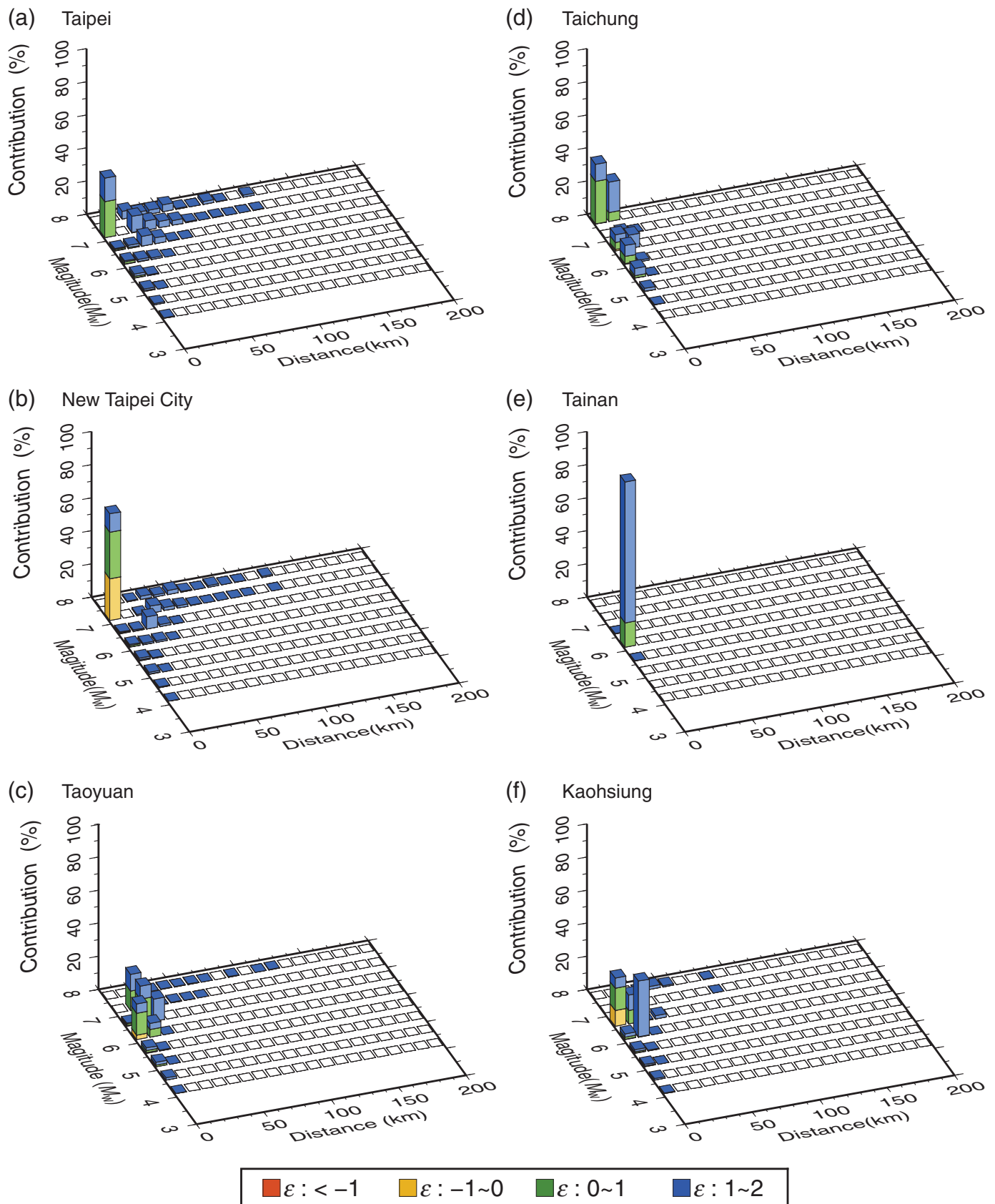


▲ **Figure 3.** Seismic source disaggregation for (a) PGA, (b) spectral acceleration at 0.3 s (SA-0.3), and (c) spectral acceleration at 1.0 s (SA-1.0) for the six cities according to the TEM PSHA2015.

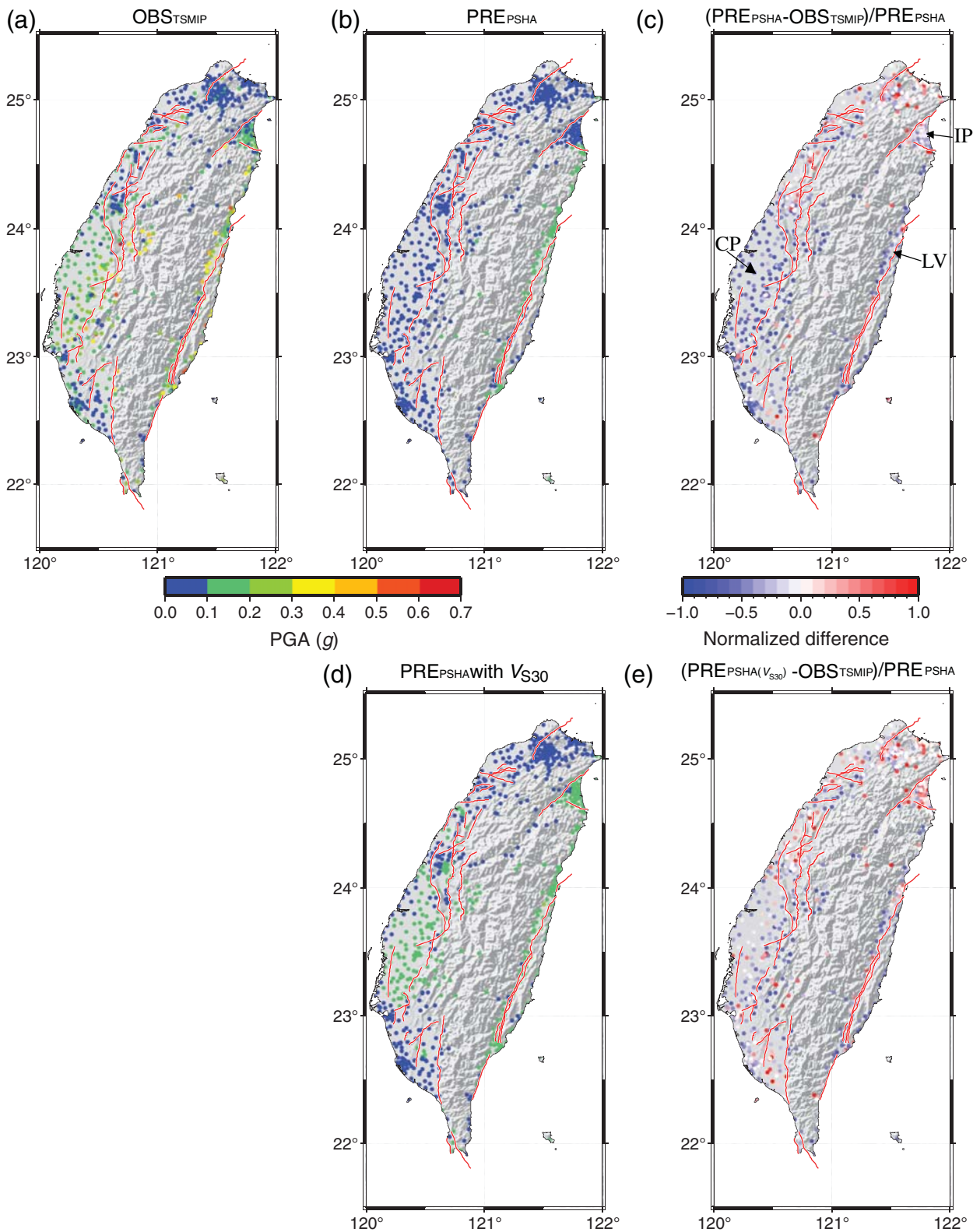
this time period, except for the 1999 Chi-Chi mainshock that ruptured on the Chelungpu fault, other earthquakes did not produce any surface rupture and thus could not be aligned with any seismogenic structure source. In other words, the seismic hazard in the past nearly 40 years in Taiwan, except for the 1999 Chi-Chi earthquake, was caused by areal or subduction zone sources. To examine the practicability of the TEM PSHA2015, we performed PGA predictions from the areal and subduction zone sources of the PSHA model and compared them with the observed data, while excluding the data from the Chi-Chi mainshock. This catalog was declustered to avoid bias caused by aftershocks and swarm events, which are dependent on one another. The recorded PGA of the events after declustering was used for the examination.

According to the Poisson process, a hazard map with a 475-year return period has a 10% PoE in 50 years. Thus, during the 23-year period of 1993–2015, the largest observed PGA recorded at each site was assumed to have an annual rate of  $1/23$ , and a corresponding 63% PoE in an observation period ( $63\% = 1 - 10^{-0.4343}$ ) was expected. Figure 5b shows the PSHA model induced by areal sources and subduction zone sources for a 63% PoE in 23 years. The maximum observed PGA of the areal sources and subduction zone sources in 23 years shows a higher level in the following regions: the coastal plain (CP), Ilan plain (IP), and longitudinal valley (LV) (Fig. 5a). The observed PGA in these regions was  $\sim 0.15$ – $0.30g$ . The hazard map of these areal and subduction zone sources for a 63% PoE in the 23-year period exhibited a lower PGA (less than  $0.1g$ ) in the plains of western Taiwan and the IP (Fig. 5b). The predicted PGA in the LV was  $\sim 0.2g$ . To quantify the comparison between the observed maximal PGA and the predicted value, we compared the normalized PGA difference between them, defined as the difference between the predicted and observed maximal PGAs, divided by the observed value. Figure 5c presents the residual between the observed PGA (Fig. 5a) and the predicted PGA without considering  $V_{S30}$  (i.e., the TEM PSHA2015 model, shown in Fig. 5b). The result shows that 70% of the observed PGAs are higher than those predicted from the PSHA model. The normalized PGA difference is  $\pm 0.5$  on average. The most underpredicted sites of the PSHA model are in CP and in IP, because 85% of the sites in CP and 70% of those in IP have a lower estimated PGA. In CP, the predicted PGAs are generally 0.5–1.0 times the observed PGAs, and in IP, the predicted PGAs are generally 0.1–0.3 times the observed values. Note that the TEM PSHA2015 was computed for bedrock sites ( $V_{S30} = 760$  m/s) to provide a basis for crucial infrastructures. The significant deviation in the PGA between the observation and prediction in the CP could imply the impact of site effect, rather than sources (e.g., magnitude) or ray path (e.g., distance).

Figure 5d shows the map considering site amplification. The values of  $V_{S30}$  at stations were measured by the suspension PS logging system (Kuo *et al.*, 2012). The GMPEs adopted in the PSHA model in this study consider the  $V_{S30}$  at every site. The predicted PGA considering the  $V_{S30}$  was  $\sim 0.2g$  in the CP, IP, and LV. In northern and southwestern Taiwan, the PGA was



▲ **Figure 4.** Magnitude–distance–epsilon ( $\epsilon$ ) disaggregation for PGA according to the TEM PSHA2015 (Wang *et al.*, 2016) for the six cities (a) Taipei, (b) New Taipei City, (c) Taoyuan, (d) Taichung, (e) Tainan, and (f) Kaohsiung with a return period of 475 years (e.g., 10% PoE in 50 years).



▲ **Figure 5.** Comparison of the observed maximal PGA for 1993–2015 and predicted PGA of probabilistic seismic-hazard analysis (PSHA) with a 63% PoE over 23 years. (a) Observed maximal PGA recorded by the Taiwan Strong Ground Motion Network during 1993–2015. (b) Predicted PGA of the PSHA according to shallow areal sources and subduction zone sources for bedrock sites ( $V_{S30} = 760$  m/s). (c) Normalized PGA difference between the observed maximal PGA and the predicted PGA. The normalized PGA difference is defined as the difference between the predicted and observed maximal PGAs divided by the observed maximal PGA for bedrock sites ( $V_{S30} = 760$  m/s). (d) Predicted PGA considering the  $V_{S30}$  of the sites. (e) Normalized PGA difference between the observed maximal PGA and the predicted PGA considering  $V_{S30}$ . The coastal plain, Ilan plain, and longitudinal valley are denoted by CP, IP, and LV, respectively.

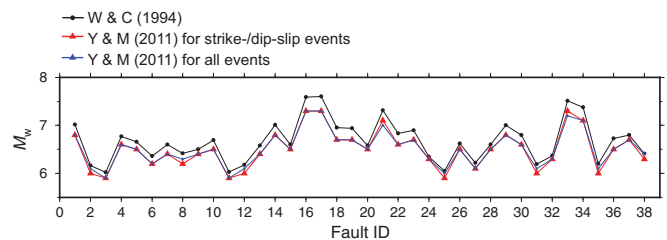
less than  $0.1g$ ; in these cases, the predicted PGA was nearer to the observed PGA. Figure 5e presents the residuals between the observed PGA (Fig. 5a) and predicted PGA considering  $V_{S30}$  (Fig. 5d). The average normalized PGA difference is  $\pm 0.3$  after considering  $V_{S30}$ . The sites with predicted PGAs lower than the observed values decrease to 56%, including 74% and 35% in CP and IP, respectively. The normalized PGA difference is  $-0.1$  to  $-0.3$  in CP. In IP, the normalized PGA difference is 0.2–0.6 times higher than the observed ones, suggesting an over site amplification in  $V_{S30}$  for IP. Overall, the predicted PGA considering  $V_{S30}$  was more consistent with the observed PGAs, indicating the applicability of the areal and subduction zone source parameters and the importance of the site effect for PSHA. The deviation between the observed and the predicted PGAs from the PSHA model in CP, LV, and IP suggests a site amplification factor for the plain areas might need to be reexamined to make the site condition more reliable. In addition, the observation time of seismic catalog adopted in this study (i.e., 23 years) could be too short to be utilized in confirming the predicted hazard model.

## UNCERTAINTY QUANTIFICATION WITH TORNADO DIAGRAMS

Compared with the rupture recurrence interval of the faults (generally several hundreds or thousands of years), the observed historical seismic record is relatively short. It is difficult to utilize this observed historical data in characterizing the overall earthquake behavior of the faults. To determine the sensitivity of the seismogenic structure sources in the TEM PSHA2015, tornado diagrams were employed to estimate the impact of the uncertainties on hazard assessment using the source model.

The parameters of the seismogenic structures used in the TEM PSHA2015 include the maximum magnitude, fault-slip rate, and dip angle of the fault plane. The maximum magnitude of the 38 seismogenic structures in the TEM PSHA2015 was estimated from the scaling laws of Wells and Coppersmith (1994). Yen and Ma (2011) investigated earthquakes (moment magnitude [ $M_w$ ] 4.6–8.9), mostly from the Taiwan orogenic belt, to obtain a scaling relationship between the fault area and magnitude. The difference in the maximum magnitude determinations of the 38 seismogenic structures (Table 1) from these two scaling relationships was  $\sim 0.2$ , as shown in Figure 6. Therefore, for maximum magnitude uncertainties from seismogenic structure sources, we estimated the hazard deviation induced by the uniform uncertainty as  $\pm 0.2$  of the maximum magnitude.

The large deviation of rock dating and the difficulty in determining the time of the previous earthquake rupture from each seismogenic structure caused high uncertainty in the estimation of the slip rate. Shyu et al. (2016) compiled a complete database for the parameters of the fault sources (i.e., seismogenic structures), including the slip-rate uncertainty of each seismogenic structure. The variability on the hazard induced by the uncertainty in the fault sources was analyzed considering the upper and lower bounds of the slip rates com-



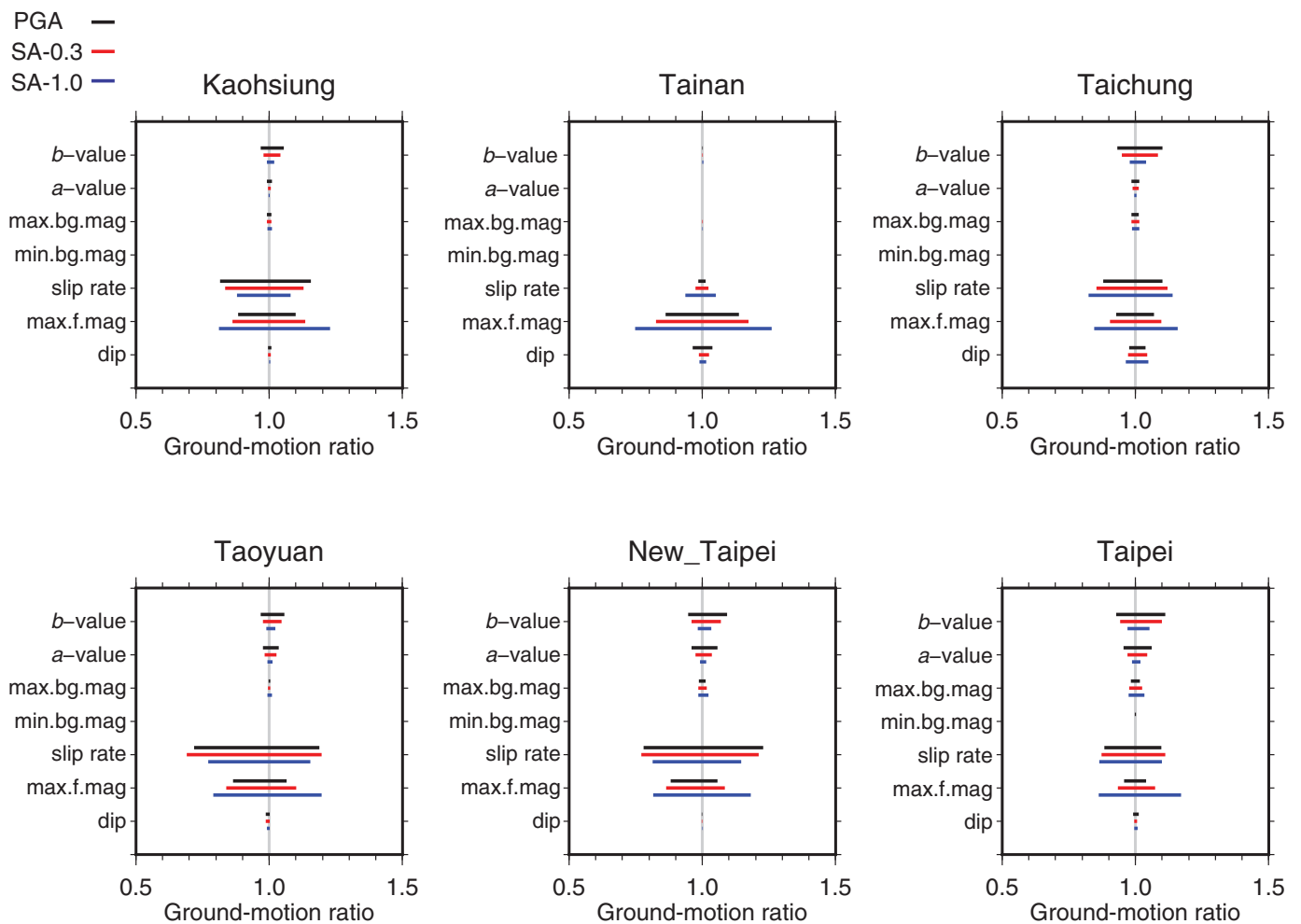
▲ **Figure 6.** Maximum magnitudes of the 38 seismogenic structures evaluated by three scaling laws. The values estimated using the scaling laws of Wells and Coppersmith (1994), Yen and Ma (2011) for dip-slip or strike-slip events, and Yen and Ma (2011) for all events are denoted by W & C (1994), Y & M (2011), and Y & M (2011), respectively.

plied by Shyu et al. (2016). For the dip of the fault sources, we considered a 10% variation of the dip angle (Table 1) for the investigation.

Tornado diagram analysis is a well-accepted tool for the sensitivity analysis of PSHA models (Field et al., 2014). The tornado diagram depicts the approximate effect of each uncertain input on the quantity of interest in the form of a horizontal bar chart that resembles a tornado in profile, hence the name. It was first used by Porter et al. (2002) in earthquake engineering. Figure 7 shows the deviation of the PGA values, referring to the parameter uncertainties of the fault sources. The hazard deviation is shown in the ground-motion ratio, which is defined as the ratio of the ground motion induced by the parameters' boundary values to that induced by the mid-range. The diagrams suggest that the PSHAs in the six cities were sensitive to the slip rate and maximum magnitude. The influence of these two factors was greater than that of the dip of the fault geometry. The change of dip with a 10% variation (Table 1) had a lower effect on the hazard analysis. The 0.2 scale difference in the fault rupture maximum magnitude resulted in PGAs of 0.87–1.13, 0.82–1.16, and 0.75–1.26 times the values of the original PGA, SA-0.3, and SA-1.0, respectively, indicating that the SA-1.0 was more sensitive than PGA or SA-0.3 for the maximum magnitude. In addition to the fault rupture maximum magnitude, the ground-motion uncertainties from the slip rates were 0.72–1.22, 0.7–1.2, and 0.78–1.14 times those of the original PGA, SA-0.3, and SA-1.0, respectively. The slip-rate uncertainties and maximum magnitude variation had equal effects on the hazard deviation in the studied cities, except for Tainan, where the ground motion is influenced more by the uncertainties in the maximum magnitudes than by those in the slip rate. This might be due to the densely populated fault sources near Tainan city.

The variation of the ground motion induced by the uncertainties in the areal source parameters (i.e.,  $a$ - and  $b$ -values as well as the maximum and minimum magnitudes applied for the upper- and lower-bound magnitudes of the truncated Gutenberg–Richter [G-R] law) was also analyzed. In the TEM PSHA2015, the lower-bound  $M_w$  of earthquakes for areal sources was considered to be 4.0. During the instrumental history of





▲ **Figure 7.** Tornado diagrams comparing the changes in the  $a$ - and  $b$ -values, maximum magnitudes of areal sources (max.bg.mag), minimum magnitudes of areal sources (min.bg.mag), slip rates, maximum magnitudes (max.f.mag), and dips of seismogenic structures in the six cities. The changes in the variables corresponding to the parameter deviation for seismogenic structures and shallow areal sources are shown in Tables 1 and 2, respectively. The black, red, and blue bars indicate the corresponding changes for PGA, SA-0.3 s, and SA-1.0 s, respectively, for a return period of 475 years (e.g., 10% PoE in 50 years). The ground-motion ratio is defined as the ratio of the deviated ground motion to the ground motion of TEM PSHA2015.

Taiwan seismicity since 1973, the recorded maximal magnitude from an areal source was the 5 September 1996  $M_w$  6.96 south-east offshore Taiwan earthquake, as denoted in Figure 1c. Thus, we accordingly consider the upper-bound  $M_w$  to be 6.96 for areal sources. The maximum  $M_w$  of the earthquakes in the areal sources had more influence on the hazard than the minimum magnitude. The  $\pm 0.2$  changes in the minimum  $M_w$  from 3.8 to 4.2 had an insignificant influence on the PGA values (Fig. 7). The  $a$ - and  $b$ -values of the areal sources have a greater influence on the hazard map than the maximum  $M_w$  of the areal sources (Fig. 7). For the  $b$ -values of the 28 regions in Taiwan, we noticed that some regions have too little seismicity to give good statistics for the  $b$ -value. To avoid overzoning and insufficient data in some individual regions, and to apply the experience learned from other national seismic-hazard maps in Japan and New Zealand, which used a uniform  $b$ -value for the whole nation, we developed a G-R law for the  $b$ -value from the whole of Taiwan, and used

this uniform  $b$ -value (1.07) for the 28 areal sources. The regression of the overall background seismicity in Taiwan was assessed as 1.07 with a deviation of  $\pm 0.053$  (Table 2). The  $a$ -value, representing the activity of shallow-background seismicity, was retrieved from each areal source according to the fixed  $b$ -value. The deviations of the  $a$ -values ranged from 0.047 to 0.201, resulting in 0.95–1.06-fold ground motions. The hazard was 0.92–1.10 times that of the original PGA according to the  $b$ -values, which was slightly greater than the  $a$ -value deviations. In the central Taiwan city, Taichung, and the northern cities (Taipei and New Taipei City), the contributions of the  $b$ -values for areal seismic sources were more significant than those of the  $a$ -values. In contrast, the evaluated hazards in the southern Taiwan cities of Kaohsiung and Tainan were less sensitive to the areal source parameters. Comparing the dominant factors in different hazard periods revealed that SA-1.0 and SA-0.3 were more sensitive to the maximum magnitude of faults than PGA.

Area	<i>a</i> -Value	<i>b</i> -Value
S01	3.69 (±0.103)	1.07 (±0.053)
S02	4.01 (±0.102)	1.07 (±0.053)
S03	3.66 (±0.117)	1.07 (±0.053)
S04	3.17 (±0.198)	1.07 (±0.053)
S05A	3.57 (±0.201)	1.07 (±0.053)
S05B	4.32 (±0.052)	1.07 (±0.053)
S06	4.63 (±0.052)	1.07 (±0.053)
S07	4.72 (±0.087)	1.07 (±0.053)
S08A	4.14 (±0.061)	1.07 (±0.053)
S08B	3.74 (±0.171)	1.07 (±0.053)
S09	3.98 (±0.144)	1.07 (±0.053)
S10	4.80 (±0.172)	1.07 (±0.053)
S11	4.63 (±0.082)	1.07 (±0.053)
S12	4.84 (±0.048)	1.07 (±0.053)
S13	4.37 (±0.136)	1.07 (±0.053)
S14A	4.34 (±0.163)	1.07 (±0.053)
S14B	4.92 (±0.047)	1.07 (±0.053)
S14C	4.79 (±0.123)	1.07 (±0.053)
S15	5.33 (±0.076)	1.07 (±0.053)
S16	5.56 (±0.108)	1.07 (±0.053)
S17A	5.21 (±0.053)	1.07 (±0.053)
S17B	4.42 (±0.141)	1.07 (±0.053)
S18A	4.91 (±0.055)	1.07 (±0.053)
S18B	4.58 (±0.080)	1.07 (±0.053)
S19A	5.16 (±0.134)	1.07 (±0.053)
S19B	4.60 (±0.101)	1.07 (±0.053)
S20	4.53 (±0.110)	1.07 (±0.053)
S21	5.12 (±0.142)	1.07 (±0.053)

## DISCUSSION AND CONCLUSIONS

The disaggregation analysis shows that the areal sources and seismogenic structure sources were the most dominant sources for the TEM PSHA2015. Therefore, reliable crustal source parameters are critical to hazard analysis, specifically for short-period ground motion (e.g., PGA). The subduction zone sources contributed substantially to SA-1.0, in addition to PGA, and thus should be addressed and given special attention for northern Taiwan.

Taipei, located in northern Taiwan, is the economic and political center of Taiwan. Since 1900, the only major intraplate earthquake that brought damage to the city was the 1909 Taipei earthquake (CWB historical earthquake catalog), even though the city was not heavily populated at that time. According to Kanamori *et al.* (2012), the Taipei earthquake was a relatively deep (50–100 km) intraplate earthquake that occurred within the subducting Philippine Sea plate beneath Taipei with an estimated  $M_w$  of  $7.0 \pm 0.3$ . Liao *et al.* (2016) simulated the

Interplate Earthquakes				
Source	Dip (°)	$M_w$	Area (km <sup>2</sup> )	Slip Rate (mm/yr)
T01A	20 (±2)	8.0 (±0.2)	14,188	40 (±10)
T02A	24 (±2)	7.5 (±0.2)	4280.4	8 (±4)
T02B	24 (±2)	7.5 (±0.2)	3736.1	8 (±4)
T02C	24 (±2)	7.5 (±0.2)	4404.8	8 (±4)
Intraplate Earthquakes				
Source	$M_0$	<i>a</i> -Value	<i>b</i> -Value	$M_u$
NP1	5.0	4.20	0.91	7.7 (±0.2)
NP2	5.0	3.57	0.80	7.7 (±0.2)
NP3	5.0	3.54	0.87	7.7 (±0.2)
NP4	5.0	2.68	0.73	7.8 (±0.2)
NP5	5.0	3.07	0.94	7.8 (±0.2)
NP6	5.0	3.26	0.96	7.8 (±0.2)
NP7	5.0	2.46	0.73	7.8 (±0.2)
NP8	5.0	3.73	1.04	7.8 (±0.2)
NP9	5.0	3.61	0.91	7.8 (±0.2)
SP1	5.0	3.07	0.76	7.7 (±0.2)
SP2	5.0	3.76	0.83	7.8 (±0.2)
SP3	5.0	3.72	0.88	7.8 (±0.2)

$M_w$  represents the maximal magnitudes for interplate earthquakes, and  $M_0$  and  $M_u$  represent the minimal and maximal magnitudes for intraplate earthquakes, respectively.

ground motions induced by this earthquake in the metropolitan area of Taipei, suggesting a possible significantly long *P*-wave shaking duration. The severe threat of the intraplate earthquake indicated by seismic source disaggregation suggests that we should focus further on the intraplate sources in addition to the seismogenic structure near Taipei, such as the Shanchiao fault (ID 1). Our analysis did not show a significant threat from a subduction zone interplate earthquake. However, this result strongly depends on the justification of the possible maximum magnitude of the interplate earthquakes from the Ryukyu and Manila subduction zones. This aleatoric uncertainty in the possible  $M_{max}$  of the subduction zone system left this concern unresolved.

Nevertheless, the comparison of the observed PGA with the expected PGA for a 63% PoE over 23 years indicates a high correspondence after considering the  $V_{S30}$  for each site, confirming the applicability of the areal and subduction zone source parameters adopted in the TEM PSHA2015. Site amplification factors, such as  $V_{S30}$ , are crucial for PSHA application to assess the shaking on the ground surface. Although the TEM PSHA2015 did not apply this factor, relative information (e.g.,  $V_{S30}$ , transfer functions of sites, and response spectra) could be incorporated in the next-generation hazard map.


A large dataset of the observation is necessary for examining the practicability of the PSHA model. However, the time

window of available observations is usually short, which could result in lower statistical power for the testing of the PSHA model (Mak *et al.*, 2014). Our comparison between observation and prediction was made only for areal and subduction sources, as only one earthquake, the 1999 Chi-Chi earthquake, was associated with an identified fault source since the beginning of the more complete seismic catalog after 1973. The historical damaging earthquakes prior to 1973 (compiled historical damaging earthquakes were after 1600 from CWB) have not yet been fully examined for their possible individual associations with seismogenic structure sources or areal sources. The practicability of the TEM PSHA2015 to the seismogenic source structure was therefore still difficult to determine. Further studies on historical damaging earthquakes could help to improve this investigation.

The tornado diagram shows that the PSHA calculation is most sensitive to the slip rate and maximum magnitude of the seismogenic structure sources. In southern Taiwan, due to the densely populated fault sources, the maximum magnitude is more sensitive than the slip rate. As the TEM PSHA2015 considered only individual fault sources, no multiple-segmented fault sources of neighboring faults were considered. The multiple-fault segmentations from neighboring fault sources will yield larger maximum magnitudes, which was not yet considered in the model and requires further attention for future PSHA analysis, especially for southern Taiwan. Of the areal source parameters, the *b*-value has a greater influence on the PSHA than the *a*-value, minimum magnitude, and maximum magnitude of the areal sources. The comparison of the generally lower predicted PGA from PSHA (after  $V_{S30}$  correction) to the observation from areal sources suggests that the hazard from areal sources in PSHA is underestimated. The *a*- and *b*-value estimations still need further justification.

A detailed investigation of the epistemic uncertainty in the TEM PSHA2015 provides practical information for seismic-hazard mitigation and is also important for the next-generation PSHA (e.g., logic tree, site corrections, and fault segmentations). The analysis performed in this study is essential to understand which models/parameters control PSHA. The TEM PSHA2015 along with this disaggregation analysis provides crucial information for governmental assessment of the hazards of specific sites, particularly for metropolitan cities and other critical facility sites.

## DATA AND RESOURCES

The earthquake catalog used in this study were provided by the Central Weather Bureau of the Taiwan Government and can not be released to the public. The seismogenic structure sources data used in this article came from published sources listed in the reference (Shyu *et al.*, 2016). The plots were made using the Generic Mapping Tools v.4.5.9 ([www.soest.hawaii.edu/gmt](http://www.soest.hawaii.edu/gmt), last accessed October 2014; Wessel and Smith, 1998). Figures and tables are reprinted (adapted or reprinted in part) with permission from Wang *et al.* (2016). 

## ACKNOWLEDGMENTS

We thank the Global Earthquake Model (GEM) for developing the open source software OpenQuake, with which this study was conducted. We thank the Central Weather Bureau for providing the ground-motion data used in this study. The suggestions and comments from the Taiwan Earthquake Model (TEM) committee members were also crucial to this study. This research was supported by the Taiwan Earthquake Research Center (TEC) funded through Ministry of Science and Technology (MOST), formerly the National Science Council (NSC) with project Grant Numbers MOST 103-2116-M-008-008-MY3, MOST 104-2625-M-008-014-MY2, MOST 105-2811-M-008-028, and MOST 105-2119-M-006-016. The TEC Contribution Number for this article is 00200.

## REFERENCES

- Albarelo, D., and V. D'Amico (2008). Testing probabilistic seismic hazard estimates by comparison with observations: An example in Italy, *Geophys. J. Int.* **175**, no. 3, 1088–1094, doi: [10.1111/j.1365-246X.2008.03928.x](https://doi.org/10.1111/j.1365-246X.2008.03928.x).
- Bazzurro, P., and C. A. Cornell (1999). Disaggregation of seismic hazard, *Bull. Seismol. Soc. Am.* **89**, no. 2, 501–520.
- Beauval, C., P.-V. Bard, and J. Douglas (2010). Comment on “Test of Seismic Hazard Map from 500 Years of Recorded Intensity Data in Japan” by Masatoshi Miyazawa and Jim Mori, *Bull. Seismol. Soc. Am.* **100**, no. 6, 3329–3331, doi: [10.1785/0120100065](https://doi.org/10.1785/0120100065).
- Beauval, C., P.-Y. Bard, S. Hainzl, and P. Guéguen (2008). Can strong-motion observations be used to constrain probabilistic seismic-hazard estimates? *Bull. Seismol. Soc. Am.* **98**, 509–520.
- Beauval, C., and O. Scotti (2004). Quantifying sensitivities of PSHA for France to earthquake catalog uncertainties, truncation of ground-motion variability, and magnitude limits, *Bull. Seismol. Soc. Am.* **94**, no. 5, 1579–1594, doi: [10.1785/012003246](https://doi.org/10.1785/012003246).
- Chen, C.-H., J.-P. Wang, Y.-M. Wu, C.-H. Chan, and C.-H. Chang (2013). A study of earthquake inter-occurrence times distribution models in Taiwan, *Nat. Hazards* **69**, no. 3, 1335–1350 doi: [10.1007/s11069-012-0496-7](https://doi.org/10.1007/s11069-012-0496-7).
- Cornell, C. A. (1968). Engineering seismic risk analysis, *Bull. Seismol. Soc. Am.* **58**, no. 5, 1583–1606.
- Field, E. H., G. P. Biasi, P. Bird, T. E. Dawson, K. R. Felzer, D. D. Jackson, K. M. Johnson, T. H. Jordan, C. Madden, A. J. Michael, *et al.* (2014). Uniform California earthquake rupture forecast, version 3 (UCERF3)—The time-independent model, *Bull. Seismol. Soc. Am.* **104**, no. 3, 1122–1180.
- Gardner, J. K., and L. Knopoff (1974). Is the sequence of earthquakes in southern California, with aftershocks removed, Poissonian? *Bull. Seismol. Soc. Am.* **64**, no. 5, 1363–1367.
- Giardini, D., G. Grünthal, K. M. Shedlock, and P. Zhang (1999). The GSHAP global seismic hazard map, *Ann. Geophys.* **42**, no. 6, doi: [10.4401/ag-3784](https://doi.org/10.4401/ag-3784).
- Giner, J., S. Molina, and P. Jauregui (2002). Advantages of using sensitivity analysis in seismic hazard assessment: A case study of sites in southern and eastern Spain, *Bull. Seismol. Soc. Am.* **92**, no. 2, 543–554, doi: [10.1785/0120000299](https://doi.org/10.1785/0120000299).
- Japan Seismic Hazard Information (J-SHIS) (2015). Available at <http://www.j-shis.bosai.go.jp/map/?lang=en> (last accessed March 2016).
- Kanamori, H., W.-H. Lee, and K.-F. Ma (2012). The 1909 Taipei earthquake—Implication for seismic hazard in Taipei, *Geophys. J. Int.* **191**, no. 1, 126–146, doi: [10.1111/j.1365-246X.2012.05589.x](https://doi.org/10.1111/j.1365-246X.2012.05589.x).
- Kuo, C.-H., K.-L. Wen, H.-H. Hsieh, C.-M. Lin, T.-M. Chang, and K.-W. Kuo (2012). Site classification and  $V_{S30}$  estimation of free-field TSMIP stations using the logging data of EGDT, *Eng. Geol.* **129**, 68–75, doi: [10.1016/j.enggeo.2012.01.013](https://doi.org/10.1016/j.enggeo.2012.01.013).

- Liao, Y.-W., Y.-T. Yen, S.-J. Lee, and K.-F. Ma (2016). Ground motion simulation of the 1909 Taipei earthquake, *Terr. Atmos. Ocean. Sci.* **72**, no. 3, 415–430, doi: [10.3319/TAO.2016.03.02.01\(TEM\)](https://doi.org/10.3319/TAO.2016.03.02.01(TEM)).
- Lin, P.-S. (2009). Ground-motion attenuation relationship and path-effect study using Taiwan data set, *Ph.D. Dissertation*, Institute of Geophysics, National Central University, Chung-Li, Taiwan (in Chinese).
- Lin, P.-S., and C.-T. Lee (2008). Ground-motion attenuation relationships for subduction-zone earthquakes in northeastern Taiwan, *Bull. Seismol. Soc. Am.* **98**, no. 1, 220–240, doi: [10.1785/0120060002](https://doi.org/10.1785/0120060002).
- Mak, S., R. A. Clements, and D. Schorlemmer (2014). The statistical power of testing probabilistic seismic-hazard assessments, *Seismol. Res. Lett.* **85**, no. 4, 781–783, doi: [10.1785/0220140012](https://doi.org/10.1785/0220140012).
- Mak, S., and D. Schorlemmer (2016). A comparison between the forecast by the United States National Seismic Hazard Maps with recent ground-motion records, *Bull. Seismol. Soc. Am.* **106**, no. 4, 1817–1831, doi: [10.1785/0120150323](https://doi.org/10.1785/0120150323).
- Miyazawa, M., and J. Mori (2009). Test of seismic hazard map from 500 years of recorded intensity data in Japan, *Bull. Seismol. Soc. Am.* **99**, no. 6, 3140–3149, doi: [10.1785/0120080262](https://doi.org/10.1785/0120080262).
- Porter, K. A., J. L. Beck, and R. V. Shaikhutdinov (2002). Sensitivity of building loss estimates to major uncertain variables, *Earthq. Spectra* **18**, no. 4, 719–743.
- Rebez, A., and D. Slejko (2000). Sensitivity analysis on the input parameters in probabilistic seismic hazard assessment, *Soil Dynam. Earthq. Eng.* **20**, no. 5, 341–351, doi: [10.1016/S0267-7261\(00\)00082-8](https://doi.org/10.1016/S0267-7261(00)00082-8).
- Seismic Hazard Harmonization in Europe (SHARE) (2013). Available at <http://www.share-eu.org/node/90> (last accessed March 2016).
- Senior Seismic Hazard Analysis Committee (1997). Recommendations for Probabilistic Seismic Hazard Analysis: Guidance on Uncertainty and Use of Experts, *U.S. Nuclear Regulatory Commission, NUREG/CR-6372*.
- Shyu, J. B. H., Y. R. Chuang, Y. L. Chen, Y. R. Lee, and C. T. Cheng (2016). A new on-land seismogenic structure source database by the Taiwan Earthquake Model (TEM) project for seismic hazard analysis of Taiwan, *Terr. Atmos. Ocean. Sci.* **72**, no. 3, 311–323, doi: [10.3319/TAO.2015.11.27.02\(TEM\)](https://doi.org/10.3319/TAO.2015.11.27.02(TEM)).
- Stein, S., B. D. Spencer, and E. M. Brooks (2015). Metrics for assessing earthquake-hazard map performance, *Bull. Seismol. Soc. Am.* **105**, no. 4, 2160–2173, doi: [10.1785/0120140164](https://doi.org/10.1785/0120140164).
- Stirling, M., and M. Gerstenberger (2010). Ground motion-based testing of seismic hazard models in New Zealand, *Bull. Seismol. Soc. Am.* **100**, 1407–1414.
- Tasan, H., C. Beauval, A. Helmstetter, A. Sandikkaya, and P. Guéguen (2014). Testing probabilistic seismic hazard estimates against accelerometric data in two countries: France and Turkey, *Geophys. J. Int.* **198**, 1554–1571, doi: [10.1093/gji/ggu191](https://doi.org/10.1093/gji/ggu191).
- Wang, Y.-J., C.-H. Chan, Y.-T. Lee, K.-F. Ma, J. Bruce, H. Shyu, R.-J. Rau, and C.-T. Cheng (2016). Probabilistic seismic hazard assessment for Taiwan, *Terr. Atmos. Ocean. Sci.* **27**, no. 3, 325–340, doi: [10.3319/TAO.2016.05.03.01\(TEM\)](https://doi.org/10.3319/TAO.2016.05.03.01(TEM)).
- Wells, D. L., and K. J. Coppersmith (1994). New empirical relationships among magnitude, rupture length, rupture width, rupture area, and surface displacement, *Bull. Seismol. Soc. Am.* **84**, 974–1002.
- Wessel, P., and W. H. Smith (1998). New, improved version of Generic Mapping Tools released, *Eos Trans. AGU* **79**, no. 47, 579.
- Yen, Y.-T., and K.-F. Ma (2011). Source-scaling relationship for M 4.6–8.9 earthquakes, specifically for earthquakes in the collision zone of Taiwan, *Bull. Seismol. Soc. Am.* **101**, no. 2, 464–481, doi: [10.1785/0120100046](https://doi.org/10.1785/0120100046).

Yu-Ju Wang<sup>1</sup>  
Ya-Ting Lee  
Kuo-Fong Ma

Department of Earth Sciences  
National Central University Taiwan  
300 Jhongda Road, Jhongli District  
Taoyuan City 32001, Taiwan (ROC)  
[shine2530@gmail.com](mailto:shine2530@gmail.com)

Chung-Han Chan  
Earth Observatory of Singapore  
Nanyang Technological University Singapore  
N2-01A-14, 50 Nanyang Avenue  
Singapore 639798

Published Online 19 October 2016

<sup>1</sup> Also at Institute of Nuclear Energy Research, Atomic Energy Council, 1000 Wenhua Road, Jiaan Village, Longtan District, Taoyuan City 32546, Taiwan (ROC).